ACS APPLIED MATERIALS & INTERFACES

Research Article

www.acsami.org

3D Hollow Framework Silver Nanowire Electrodes for High-Performance Bottom-Contact Organic Transistors

Jiye Kim,[†] So Hee Lee,[§] Haekyoung Kim,*[,§] Se Hyun Kim,*[,‡] and Chan Eon Park*[,†]

[†]POSTECH Organic Electronics Laboratory, Department of Chemical Engineering, Pohang University of Science and Technology, 77 Cheongam-Ro, Nam-Gu, Pohang, Gyungbuk 790-784, Korea

[‡]Department of Nano, Medical and Polymer Materials, Yeungnam University, 280 Daehak-Ro, Gyungsan, Gyeongbuk 712-749, Korea

[§]School of Materials Science and Engineering, Yeungnam University, 280 Daehak-Ro, Gyungsan, Gyeongbuk 712-749, Korea

Supporting Information

ABSTRACT: We successfully fabricated high performance bottom-contact organic field-effect transistors (OFETs) using silver nanowire (AgNW) network electrodes by spray deposition. The synthesized AgNWs have the dimensions of 40−80 nm in diameter and 30−80 μm in length and are randomly distributed and interconnected to form a 3D hollow framework. The AgNWs networks, deposited by spray coating, yield an average optical transmittance of up to 88% and a sheet resistance as low as 10 ohm/sq. For using AgNWs as source/drain electrodes of OFETs with a bottom-contact configuration, the large contact resistance at the AgNWs/organic channel remains a critical issue for charge injection. To enhance charge injection, we fabricate semiconductor crystals on the AgNW using an adsorbed residual poly(*N*-vinylpyrrolidone) layer. The resulting bottom-contact OFETs exhibit high mobility up to 1.02 $cm^2/(V\ s)$ and are similar to that of the top-contact Au electrodes OFETs with low contact resistance. A morphological study shows that the pentacene crystals coalesced to form continuous morphology on the nanowires and are highly interconnected with those on the channel. These features contribute to efficient charge injection and encourage the improvement of the bottom-contact device performance. Furthermore, the large contact area of individual AgNWs spreading out to the channel at the edge of the electrode also improves device performance.

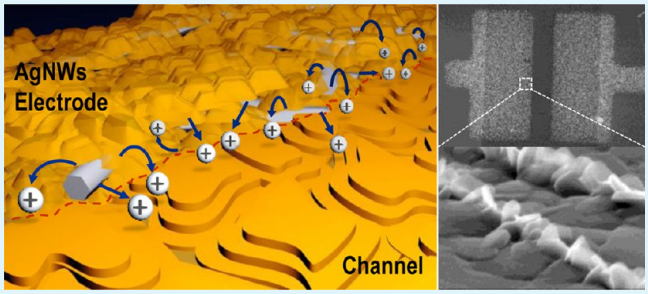

KEYWORDS: *organic field-effect transistor, silver nanowire, spray coating, bottom contact source/drain electrode, pentacene*

1. INTRODUCTION

Research on organic field-effect transistors (OFETs) has made remarkable progress, such that OFETs are now being applied in several established and/or emerging technologies, including displays, smart cards, and sensors.[1,2] Nevertheless, there are still several bottlenecks hindering the development of OFETs suitable for use as the driving units of next-generation electronic applications, which require high performance, transparency, and mechanical flexibility, as well as cheap and eco-friendly manufacturing processes. Moreover, the conductive materials used as the source, drain, and gate electrodes of an OFET should fulfill additional requirements, including high electrical conductivity and an appropriate energy match with the organic semiconductor.[3] Although metals such as gold, aluminum, and silver have been widely employed in OFETs due to their high conductivity,[3] the high cost of vacuum deposition to make thin films as well as the opaqueness of these metals are an impediment to the future progress of OFETs.

For the above reasons, recent studies have focused on the technology for the development of various solution-processed conductive materials such as poly(3,4-ethylenedioxythiophene/polystyrenesulfonate) (PEDOT:PSS), carbon nanotubes, graphene, metal grids, and metallic nanowires.[3−8] Among them, random silver nanowire (AgNW) networks have been regarded as promising candidates to replace indium tin oxide (ITO) because of their attractive electrical, thermal, and optical properties.[9−11] In contrast to common conductive materials with a dense thin film structure, AgNW networks are comprised of a three-dimensional (3D) hollow framework in which individual nanowires are connected to each other to establish an electrical pathway.[9,10] This structure allows the AgNW network film to simultaneously exhibit transparency, conductivity, and mechanical flexibility. However, if AgNW networks are used as the source/drain electrodes in bottom-contact OFETs, charge injection phenomena between the hollow AgNW network electrode and the organic semiconductor layer will play a critical role in determining the device performance. In general, the use of metal source/drain electrodes in OFETs with a bottom-contact configuration has frequently led to contact resistance arising from a carrier

Received: March 25, 2015
Accepted: June 17, 2015
Published: June 17, 2015

DOI: 10.1021/acsami.5b02610
ACS Appl. Mater. Interfaces 2015, 7, 14272−14278

injection barrier[3,12] and/or structural mismatch[13−15] at the interface between the metal electrode and organic semiconductor. The contact resistance in bottom-contact OFET has been regarded as one of the causes that degrade the device performance of OFETs.

In this study, we fabricated the high performance bottom-contact OFETs in which AgNW networks were used as the source/drain electrodes. AgNW networks were easily deposited on the 300 nm thick SiO_2/Si substrate from a AgNW-dispersed solution via normal spray coating at ambient condition. Pentacene-based bottom-contact OFETs with AgNW networks as the source/drain electrodes yielded a field-effect mobility (μ_{FET}) of up to 1.02 $cm^2/(V\ s)$, which is about 4 orders of magnitude higher than those of the bottom-contact OFETs with vacuum-deposited Ag thin film electrodes and is comparable to that of the top-contact OFETs with a vacuum-deposited Au electrode that can establish an Ohmic contact at the electrode/semiconductor interface. In addition, we investigated in detail the mechanism of charge injection between the AgNW networks and pentacene semiconductor and thereby elucidated why AgNW networks enable pentacene OFETs to achieve a high μ_{FET} value in spite of the device having a bottom-contact configuration.

2. EXPERIMENTAL SECTION

2.1. Materials and Sample Preparation. AgNWs were synthesized by reducing silver nitrate with ethylene glycol (EG) in the presence of $ZnCl_2$, $Fe(NO_3)_3{\cdot}H_2O$, and poly(*N*-vinylpyrrolidone) (PVP). A 200 mL EG solution with PVP was vigorously stirred in a 500 mL three-neck round flask. After the PVP had dissolved, $ZnCl_2$, $Fe(NO_3)_3{\cdot}H_2O$, and $AgNO_3$ were added. Then, the reaction was carried out at 130 °C for 4 h. AgNWs were obtained after washing with ethanol and DI water two or three times. The resulting AgNWs had the dimensions of 40−80 nm in diameter and 30−80 μm in length. The 0.1 wt % of the prepared AgNWs was dispersed in isopropyl alcohol (IPA).

2.2. Device Fabrication. Highly doped n-type (100) Si wafers having thermally grown SiO_2 layers of 300 nm thickness were used as the substrates. The dimethylchlorosilane-terminated polystyrene (PS-$Si(CH_3)_2Cl$, PS-brush) polymers used for the preparation of the surface-modification layers were obtained from Polymer Source Inc. PS-brush dissolved in toluene (Aldrich) was spin-coated onto SiO_2 substrates to fabricate the surface-functionalized oxide dielectrics. The resulting films were annealed at 120 °C for 60 min under a N_2 atmosphere. To remove unreacted PS-brush residue, the annealed film was rinsed with excess toluene and then sonicated in a toluene bath for 2 min. AgNW electrodes were deposited on the PS-brush-treated SiO_2 substrate by spray coating with a AgNW solution (0.1 wt %) in isopropyl alcohol (Aldrich) through a shadow mask. A 50 nm thick pentacene film was then deposited as the semiconductor layer via organic molecular beam deposition (deposition rate = 0.1−0.2 Å/s; vacuum pressure = 10^{-6} Torr; substrate temperature = 25 °C).

2.3. Characterization. The AgNW films were characterized by an atomic force microscope (AFM), sanning electron microscope (SEM), ultraviolet photoemission spectroscopy (UPS), and X-ray photoelectron spectroscopy (XPS). UPS and XPS were performed using the 4D beamline in the Pohang Accelerator Laboratory (PAL) in Korea. The Φ value was obtained using $\Phi = h\nu - E_{cutoff} + E_{Fermi}$. The $h\nu$ is the incoming photon energy (90 eV), and the −5 V bias was applied to make a clear boundary in the E_{cutoff} region. The electrical parameters of the pentacene-based OFETs were measured using a Keithley 4200 SCS in a N_2-purged glovebox. μ_{FET} and V_{th} were calculated in the saturation regime (V_D = −40 V). The C_i was measured using an Agilent 4284 precision LCR meter. 2D-GIXD experiments were performed on pentacene films at the 3C and 9A beamlines (wavelength = 1.54 Å) in the PAL.

3. RESULTS AND DISCUSSION

The AgNW investigated here was synthesized by reducing $AgNO_3$ with ethylene glycol (EG) in the presence of $ZnCl_2$, $Fe(NO_3)_3{\cdot}H_2O$, and poly(*N*-vinylpyrrolidone) (PVP). $ZnCl_2$ and PVP were used as a seeding salt and a capping agent for anisotropic growth of AgNW, respectively.[16] The resulting AgNWs had the dimension of 40−80 nm in diameter and 30−80 μm in length, respectively, yielding an aspect ratio of ca. 375−2000 (Figure 1). This aspect ratio is comparable to or

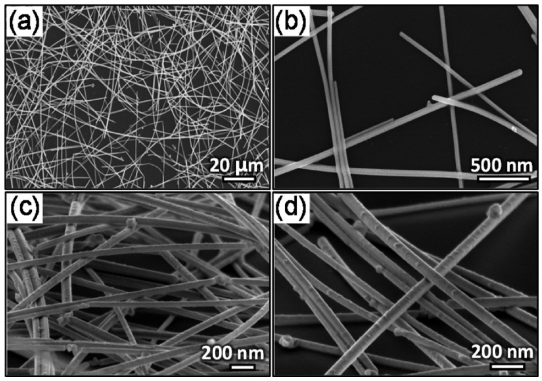

Figure 1. (a−b) SEM images of AgNWs deposited by spray coating. (c−d) Magnified SEM images of AgNWs networks. The image was taken by tilting the sample at an angle of 45°.

higher than those of previously reported AgNWs.[11,16,17] In general, the properties of conductive films consisting of a random metal nanowire network or metal mesh are the result of a trade-off between optical transmittance and electron conduction.[11,18] Use of metallic nanowires with a high aspect ratio enables electrical percolation at low density, thereby affording high optical and electrical properties. To fabricate a conductive film comprised of AgNW networks, a AgNW solution dispersed in isopropyl alcohol (0.1 wt %) was deposited on a PET substrate by commercial spray coating at ambient conditions. As a result, an average optical transmittance of 88% and a sheet resistance of 10 ohm/sq were achieved for a ca. 500 nm thick AgNW network film (Figure 2). The inset in Figure 2 shows a photograph of AgNW networks film on PET substrate. It is clear from this image that the AgNW network film shows a very high optical property.

To fabricate AgNW network source/drain electrodes for bottom-contact OFETs, AgNWs were deposited on a SiO_2/Si substrate by spray coating through a shadow mask (Figure 3a). Prior to the deposition of AgNWs, the SiO_2 dielectric surfaces

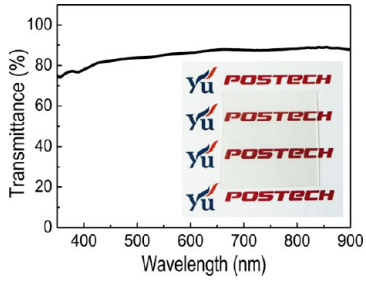

Figure 2. Transmittance of spray coated AgNWs on PET substrate. The inset shows digital camera image of a highly transparent AgNWs on PET substrate.

DOI: 10.1021/acsami.5b02610
ACS Appl. Mater. Interfaces 2015, 7, 14272−14278

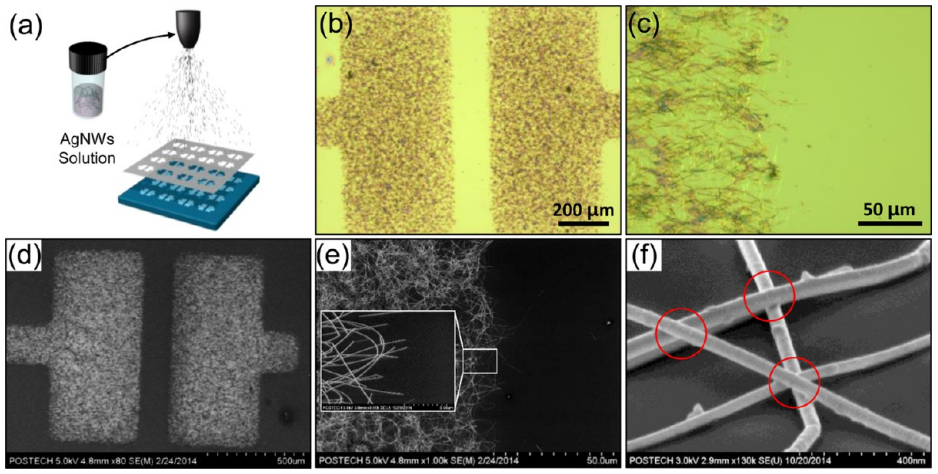

Figure 3. (a) Schematic diagram showing patterned AgNWs electrodes via spray coating through a shadow mask. The OM images of (b) patterned AgNWs electrodes and (c) channel edge. The SEM images of (d) patterned AgNWs electrodes and (e) channel edge. The inset shows that the magnified SEM image at the edge of the electrode. (f) The magnified SEM image of AgNWs networks. The image was taken by tilting the sample at an angle of 45°.

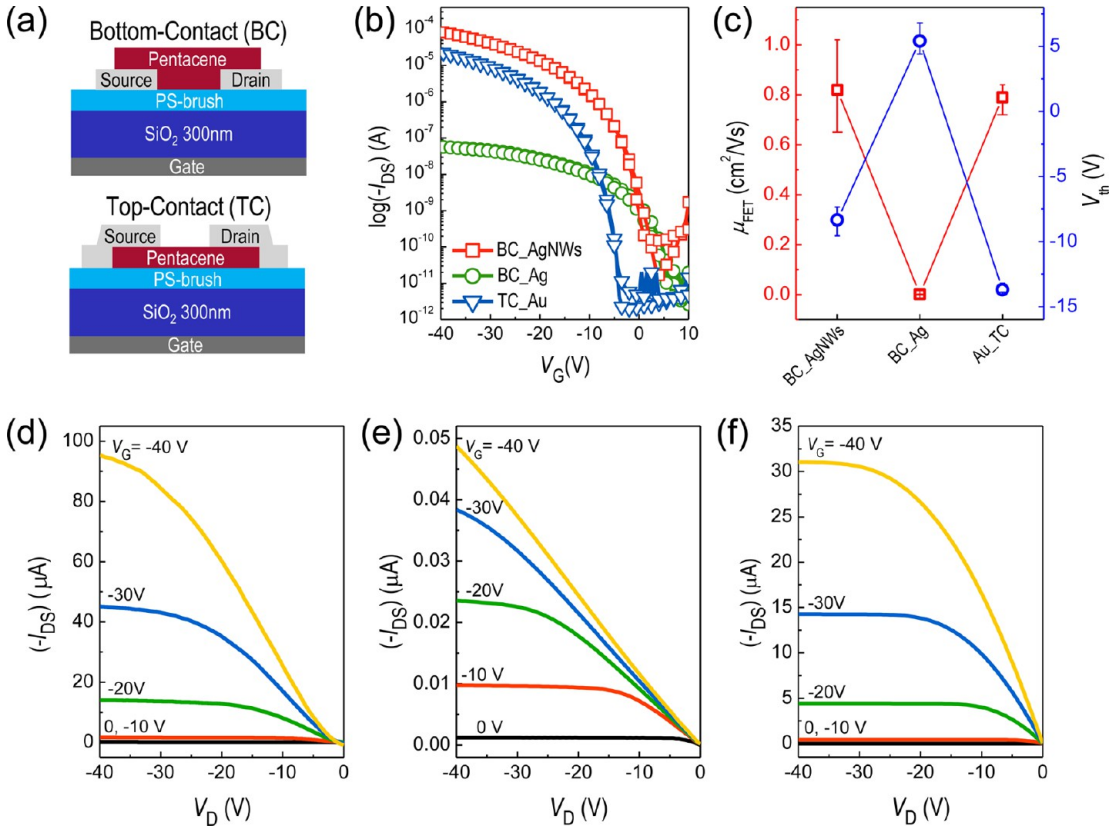

Figure 4. (a) Schematic diagram of top-contact and bottom-contact OFETs. (b) Transfer characteristics of bottom- and top-contact OFETs with AgNWs (red), Ag (green), and Au (blue) electrodes, and (c) the corresponding parameters of μ_{FET} and V_{th}. Output characteristics of OFETs with (d) bottom-contact AgNWs, (e) Ag electrodes, and (f) top-contact Au electrodes, respectively.

were modified with dimethylchlorosilane-terminated polystyrene (PS-Si$(CH_3)_2$Cl, PS-brush) to improve the interfacial properties, including the adhesion and semiconductor growth behavior.[19] As shown in Figure 3b–e, the AgNW network electrodes were distinctly patterned with a well-defined edge and clear channel region (channel length and width of 150 and 1500 μm, respectively). Higher magnification SEM images of the AgNW network electrodes showed that the AgNWs were randomly distributed and connected to each other to form a 3D hollow framework (Figure 1).

To assess the performance of the AgNW networks as OFET electrodes, the AgNW networks were compared with Ag thin film electrodes in bottom- or Au thin film electrodes in top-contact OFETs. Vacuum-deposited pentacene was used as the semiconductor, and the device structures are shown in Figure 4a. Figure 4b–f show the drain current–gate voltage (I_D–V_G) transfer and drain current–drain voltage (I_D–V_D) output

DOI: 10.1021/acsami.5b02610
ACS Appl. Mater. Interfaces 2015, 7, 14272–14278

characteristics for the bottom-contact OFETs employing AgNW networks and Ag thin films, as well as for the top-contact device based on a Au thin film. The μ_{FET} and threshold voltage (V_{th}) were determined from plots of $I_D^{1/2}$ versus V_G, according to the standard saturation regime relation $I_D = \mu_{FET}C_iW(2L)^{-1}(V_G - V_{th})^2$, where C_i is the capacitance of the gate dielectric. The electrical parameters for each OFET are summarized in Table 1. Ag thin-film-based bottom-contact

Table 1. Electrical Performances of Bottom-Contact (BC) OFETs Employing AgNWs and Ag Thin Film, and Top-Contact (TC) OFETs Employing Au Thin Film

	AgNWs (BC)	Ag (BC)	Au (TC)
average μ_{FET} ($cm^2/(V\ s)$)	0.82	9.6×10^{-4}	0.79
V_{th} (V)	−8.35 (±1.1)	5.41 (±1.2)	−13.7 (±0.4)

OFETs showed poor electrical performance, with a μ_{FET} of $\sim 10^{-4}$ $cm^2/(V\ s)$, whereas the average μ_{FET} of the top-contact Au based OFET was 0.79 $cm^2/(V\ s)$. Remarkably, the AgNW-based bottom-contact OFET yielded an average μ_{FET} of 0.82 $cm^2/(V\ s)$, with a maximum value of 1.02 $cm^2/(V\ s)$. Given that the semiconductor layer on the channel region had a similar crystalline morphology for each sample, the contact resistance at the electrode/channel interface must be the factor determining the μ_{FET} values of the devices.[3,20,21] Examination of the output characteristics of the OFETs, which provide information on contact resistance in the device, showed nonlinear curves in the linear regime of the output curve at $V_D \ll V_G$ for the AgNW-based and Ag thin film-bottom-contact OFETs (Figure 4d and e). In contrast, the Au top-contact device exhibited a linear current−voltage (I−V) dependence in the same output regime, indicating that charge injection at the electrode/channel interface obeys Ohm's law (Ohmic contact) in this device (Figure 4f).[3,22] The deviation from linearity of the output curve at $V_D \ll V_G$ for the bottom-contact OFETs can be attributed to formation of a barrier to charge injection from the electrode to the channel, generating contact resistance during device operation (Schottky contact)[23,24] (see Supporting Information for details). These findings prompt the questions: Why does the AgNW-based OFET exhibit several thousand times higher μ_{FET} than the device with a Ag thin-film electrode, even though both devices have a bottom-contact configuration? And why does the AgNW-based OFET yield a μ_{FET} comparable to that of the Au top-contact device in spite of the nonlinear I−V dependence in its output curve (Figure 4).

In general, the Schottky contact in OFETs is attributed to the difference in work function (Φ) or to a crystal structure mismatch between the semiconductor film on the electrode and the channel.[24] Therefore, it is necessary to correlate the charge injection behavior with not only the electronic structure but also the crystalline morphology at the pentacene/AgNW interface. The Φ values for the AgNW networks and Ag thin film electrodes were determined from their ultraviolet photoemission spectroscopy (UPS) energy distribution curves (Figure 5a). The as-cast AgNW sample yielded a Φ value of 6.86 eV, which was quite different from that of the Ag thin film (4.48 eV). In contrast, the Φ value (4.50 eV) of the AgNW sample after Ar-sputtering was similar to that of the Ag thin film. Since the AgNW was grown one-dimensionally by the selective adsorption of PVP polymer onto the {100} Ag crystal plane, the Φ value of the as-cast AgNW should be modified by

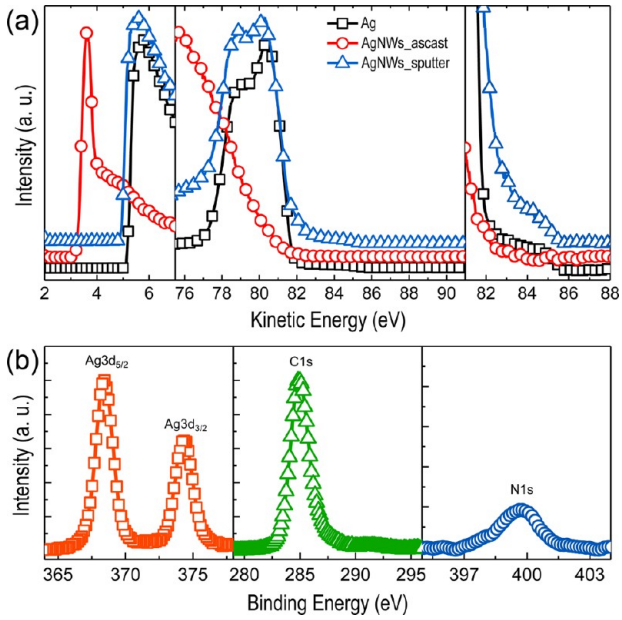

Figure 5. (a) UPS energy distribution curves for Ag thin-film, as-cast AgNWs, and Ar-sputtered AgNWs. The left side shows the secondary electron emission, and the right side shows a magnified view of the region where the Ag Fermi edge. (b) XPS spectra of Ag 3d, C 1s, and N 1s core level for AgNWs.

PVP which is adsorbed on the AgNW surface. The presence of PVP residue on the AgNW is supported by the X-ray photoelectron spectroscopy (XPS) data. As shown in Figure 5b, C 1s and N 1s peaks corresponding to PVP were clearly detected in addition to Ag 3d ones that are related to AgNW. The insulating property of PVP adsorbed on the AgNW can disturb charge carrier injection at the electrode/channel interface (see Supporting Information). Therefore, additional voltage is needed to overcome the charge injection barrier induced by the PVP, which may explain the nonlinear I−V dependence in the output curve of the AgNW-based OFETs. However, it is well-known that the introduction of organic molecules (including self-assembled monolayers[23,24] and polymers[21,25]) onto a metal electrode can control the molecular arrangement of an organic semiconductor layer deposited on the metal substrate. The growth characteristics of organic semiconductors, which mainly consist of π-conjugated planar acenes such as pentacene, will be influenced by competing interactions between the molecules and the substrate.[21,26] For example, since pure metal surfaces can strongly interact with π-conjugated systems, the molecules are adsorbed with their π-conjugation plane parallel to the surface (face-on structure). By contrast, on a dielectric surface, the interaction between π-conjugated molecules is more dominant than the molecule−substrate interaction, allowing the molecules to be normal to the surface (edge-on structure), and this molecular orientation coincides with the direction of charge transport.[19]

To elucidate the effect of crystalline morphology at the pentacene/AgNW interface on the charge carrier transport behavior, we first investigated the growth of the semiconductor layer on the pure metal and dielectric surfaces to define the structural features at the two sides. Figure 6a and b show AFM images of the pentacene films at the interface between the channel region where a hydrophobic PS-brush layer is chemisorbed on the SiO_2 dielectric and the Ag thin film electrodes. As shown in Figure 6a and b, the pentacene films on

DOI: 10.1021/acsami.5b02610
ACS Appl. Mater. Interfaces 2015, 7, 14272−14278

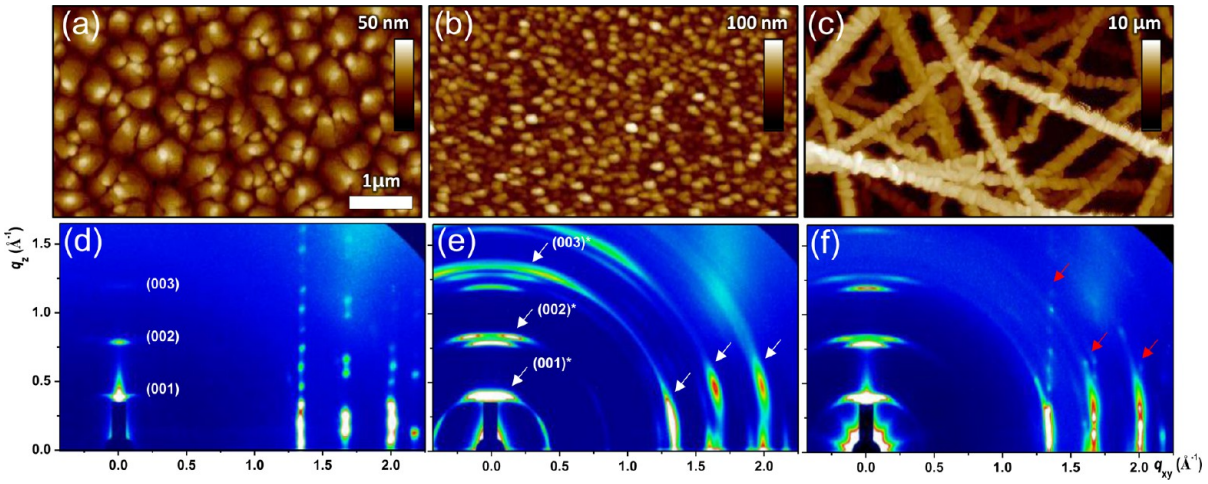

Figure 6. (a–c) AFM topographies of pentacene on (a) PS-brush treated SiO_2 dielectric, (b) Ag thin film, and (c) AgNWs, respectively. (d–f) The 2D-GIXD patterns of 50 nm thick pentacene on (d) PS-brush treated SiO_2 dielectric, (e) Ag thin film, and (f) AgNWs, respectively.

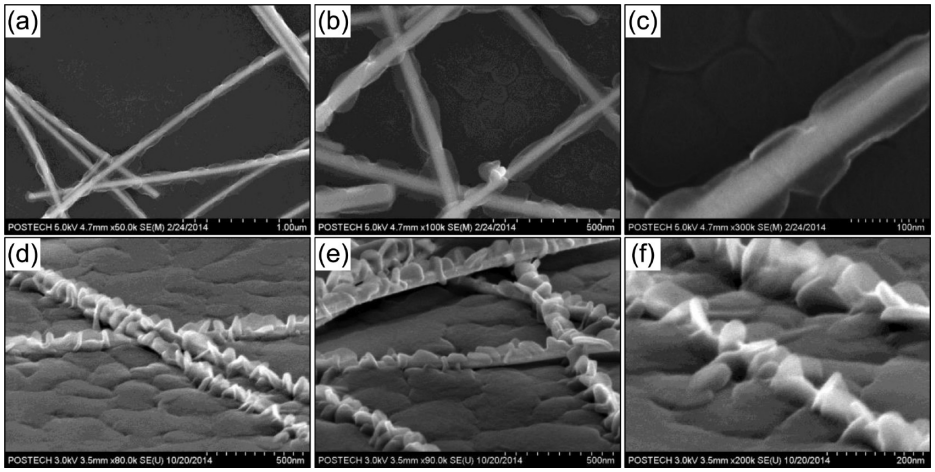

Figure 7. (a–f) Magnified SEM images of pentacene on AgNW networks. (d–f) The images were taken by tilting the sample at an angle of 45°.

the Ag thin film showed small crystals with a grain size of 50–100 nm, whereas large terrace-like pentacene crystals (~1 μm) were formed in the channel region. Further information on the molecular arrangements was obtained by examining the two-dimensional grazing-incidence X-ray diffraction (2D-GIXD) pattern of pentacene films grown on PS-brush surfaces and the Ag (Figure 6d and e). The pentacene film on the PS-brush channel, which has the same morphology on AgNW and Ag thin film electrode devices, exhibited intense (00l) crystalline reflections along the q_z axis (out-of-plane), with a d-spacing of 15.3 Å, as well as {1, ±1}, {0,2}, and {1, ±2} reflections along the q_{xy} axis (in-plane) corresponding to herringbone in-plane molecular packing. These reflections are indicative of a pseudo-orthorhombic thin-film crystalline phase. In particular, Bragg rod reflections vertically aligned with respect to the q_{xy} axis indicate that the pentacene film on the PS-brush channel had a highly oriented multilayered herringbone structure. On the other hand, the 2D GIXD patterns of the pentacene film grown on the Ag thin film is consistent with the coexistence of several crystalline phases (Figure 6e). In addition to thin-film phase reflection peaks, the presence of a triclinic bulk phase is indicated by (00l)* reflections along the q_z axis and curled peaks along the q_{xy} axis (marked by white arrows). Furthermore, both out-of-plane and in-plane reflections show scattering patterns along the Debye ring, indicating that their molecular orientations are more misaligned with respect to their own original crystal direction. The structural inhomogeneities and misorientation in the semiconductor film limited charge transport and then contributed to a degradation of the performance of the OFETs containing pentacene thin films.[27]

The morphology of the pentacene on the AgNW network electrode is shown in Figure 6c. The lateral grain size of the pentacene on the AgNW is confined to 60–120 nm due to the diameter of the underlying nanowires; this grain size is considerably less than that of the channel (~1 μm) (see Figures 6 and 7). Figure 7 shows the SEM images of pentacene on AgNW networks. In the longitudinal direction, however, pentacene grains grew along the nanowires and eventually coalesced to form continuous pentacene morphology on the nanowires (the SEM images in Figure 7a–c). The crystal growth of pentacene is significantly affected by the underlying surface. Thus, pentacene crystals grew continuously on an absorbed PVP layer on AgNWs as shown in the SEM images of Figure 7a–c. These results agree well with the 2D GIXD results. Figure 6e and f show that the 2D GIXD patterns of the pentacene film grown on AgNWs were quite different from those on the pentacene grown on the Ag thin film. Although some bulk phase peaks were observed, the pentacene crystals

DOI: 10.1021/acsami.5b02610
ACS Appl. Mater. Interfaces 2015, 7, 14272–14278

obviously contained large portions of surface-parallel molecular packing consisting of (00l) reflections along the q_z direction and vertically aligned Bragg rod reflection along the q_{xy} axis (red arrows). This structural feature of the pentacene film on the AgNW substrate can be attributed to the PVP layer adsorbed on the surface. As mentioned above, organic layers adsorbed on metal surfaces allow π-conjugated molecules to be grown with an edge-on orientation. Hence, the PVP layer on the AgNW may enhance a surface-parallel π-conjugation molecular arrangement of the pentacene film, even though a greater density of crystalline defects is present compared to the pentacene film on the channel.

Moreover, the pentacene crystals on the AgNW were highly interconnected with those on the channel. The SEM images in Figure 7d–f show a tilting view of pentacene morphology on the AgNWs. Pentacene crystals covered the boundary of the nanowire and channel region. Cross-sectional height profiles of the AFM image of the pentacene morphology on AgNWs also show the smooth edge of pentacene on AgNWs (Figure 8).

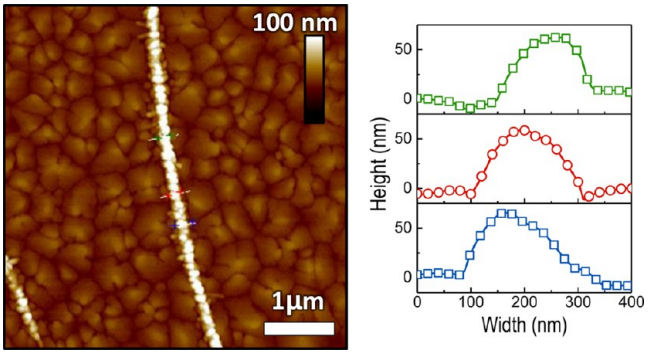

Figure 8. AFM topographies (left) and AFM cross-sectional height profiles (right) of pentacene on AgNWs.

These results indicate that the pentacene also grew at the boundary connected with grains on nanowires and channel due to the organic surface (PVP on nanowire and PS-brush on channel). Thus, the interconnected pentacene layer guarantees better charge injection and transfer from the AgNW network electrode to the channel region. Furthermore, considering the area of overlap at the electrode/channel interface where charge injection takes place in the OFETs, the morphology of this interface will be closely associated with the electrical properties of the device. As shown in the inset of Figure 3e, individual AgNWs tend to spread out to the channel at the edge of the electrode. Unlike the Ag thin film electrode with the cross section at the edge of the electrode, this morphological feature would be expected to give rise to an increase in the contact area between the electrode and channel compared to solid thin film electrodes, which would make a significant contribution to efficient charge injection in the device and hence to improved electrical performance (Figure 9).

4. CONCLUSIONS

We successfully fabricated AgNW network electrodes via ambient condition spray deposition for use in high performance bottom-contact OFETs. The resulting AgNWs, which had the dimensions of 40–80 nm in diameter and 30–80 μm in length, were randomly distributed and interconnected to form a 3D hollow framework. As a result, the AgNW network film yielded an average optical transmittance of up to 88% and a sheet

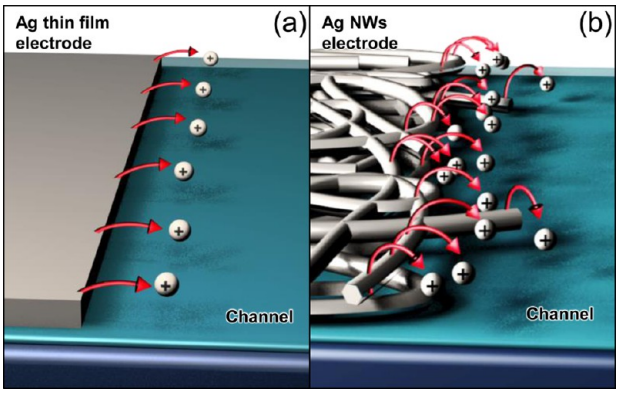

Figure 9. Schematic diagrams showing charge injection of OFETs with (a) Ag thin film and (b) AgNWs electrodes.

resistance as low as 10 ohm/sq. In particular, the pentacene-based bottom-contact OFET employing AgNW network electrodes showed a μ_{FET} about 3 orders of magnitude higher than that of the OFET with bottom-contact Ag thin film electrodes, and similar to that of the top-contact Au-based OFET. The characteristics of the various OFETs were intimately associated with the crystalline morphology at the channel/electrode interface, which affects charge carrier transport. In particular, the improved molecular orientation of the pentacene layer induced by adsorbing a PVP layer on the AgNWs enhanced the OFET performance, as did the increased contact area between the AgNWs and the pentacene layer.

■ ASSOCIATED CONTENT

Ⓢ Supporting Information

Contact resistance of metal electrodes, the injection barrier between metals and pentacene. The Supporting Information is available free of charge on the ACS Publications website at DOI: 10.1021/acsami.5b02610.

■ AUTHOR INFORMATION

Corresponding Authors

*E-mail: hkkim@ynu.ac.kr.
*E-mail: shkim97@yu.ac.kr.
*E-mail: cep@postech.ac.kr.

Notes

The authors declare no competing financial interest.

■ ACKNOWLEDGMENTS

This work was supported by a grant from the Korea Science and Engineering Foundation (KOSEF), funded by the Korean Government (MEST) (NRF-2014R1A2A1A05004993, NRF-2014R1A1A1005896, and NRF- 2012H1B8A2025602) and the Global Leading Technology Program of the Office of Strategic R&D Planning (OSP) (10042477) funded by the Ministry of Knowledge Economy, Republic of Korea.

■ REFERENCES

(1) Sekitani, T.; Zschieschang, U.; Klauk, H.; Someya, T. Flexible Organic Transistors and Circuits with Extreme Bending Stability. *Nat. Mater.* **2010**, *9*, 1015–1022.
(2) Klauk, H.; Zschieschang, U.; Pflaum, J.; Halik, M. Ultralow-Power Organic Complementary Circuits. *Nature* **2007**, *445*, 745–748.
(3) Natali, D.; Caironi, M. Charge Injection in Solution-Processed Organic Field-Effect Transistors: Physics, Models and Characterization Methods. *Adv. Mater.* **2012**, *24*, 1357–1387.

DOI: 10.1021/acsami.5b02610
ACS Appl. Mater. Interfaces 2015, 7, 14272–14278

(4) Aguirre, C. M.; Ternon, C.; Paillet, M.; Desjardins, P.; Martel, R. Carbon Nanotubes as Injection Electrodes for Organic Thin Film Transistors. *Nano Lett.* **2009**, *9*, 1457−1461.
(5) Sarker, B. K.; Liu, J.; Zhai, L.; Khondaker, S. I. Fabrication of Organic Field Effect Transistor by Directly Grown Poly(3 hexylthiophene) Crystalline Nanowires on Carbon Nanotube Aligned Array Electrode. *ACS Appl. Mater. Interfaces* **2011**, *3*, 1180−1185.
(6) Sarker, B. K.; Khondaker, S. I. Thermionic Emission and Tunneling at Carbon Nanotube-Organic Semiconductor Interface. *ACS Nano* **2012**, *6*, 4993−4999.
(7) Lee, S.; Jo, G.; Kang, S. J.; Wang, G.; Choe, M.; Park, W.; Kim, D. Y.; Kahng, Y. H.; Lee, T. Enhanced Charge Injection in Pentacene Field-Effect Transistors with Graphene Electrodes. *Adv. Mater.* **2011**, *23*, 100−105.
(8) Kang, N.; Khondaker, S. I. The Impact of Carbon sp^2 Fraction of Reduced Graphene Oxide on the Performance of Reduced Graphene Oxide Contacted Organic Transistors. *Appl. Phys. Lett.* **2014**, *105*, 223301.
(9) Xu, F.; Zhu, Y. Highly Conductive and Stretchable Silver Nanowire Conductors. *Adv. Mater.* **2012**, *24*, 5117−5122.
(10) De, S.; Higgins, T. M.; Lyons, P. E.; Doherty, E. M.; Nirmalraj, P. N.; Blau, W. J.; Boland, J. J.; Coleman, J. N. Silver Nanowire Networks as Flexible, Transparent, Conducting Films: Extremely High DC to Optical Conductivity Ratios. *ACS Nano* **2009**, *3*, 1767−1774.
(11) Hu, L.; Kim, H. S.; Lee, J.-Y.; Peumans, P.; Cui, Y. Scalable Coating and Properties of Transparent, Flexible, Silver Nanowire Electrodes. *ACS Nano* **2010**, *4*, 2955−2563.
(12) Ishii, H.; Sugiyama, K.; Ito, E.; Seki, K. Energy Level Alignment and Interfacial Electronic Structures at Organic/Metal and Organic/Organic Interfaces. *Adv. Mater.* **1999**, *11*, 605−625.
(13) Di, C.; Yu, G.; Liu, Y.; Xu, X.; Wei, D.; Song, Y.; Sun, Y.; Wang, Y.; Zhu, D.; Liu, J.; Liu, X.; Wu, D. High-Performance Low-Cost Organic Field-Effect Transistors with Chemically Modified Bottom Electrodes. *J. Am. Chem. Soc.* **2006**, *128*, 16418−16419.
(14) De Angelis, F.; Cipolloni, S.; Mariucci, L.; Fortunato, G. High-Field-Effect-Mobility Pentacene Thin-Film Transistors with Polymethylmetacrylate Buffer Layer. *Appl. Phys. Lett.* **2005**, *86*, 203505.
(15) Ihm, K.; Kim, B.; Kang, T.-H.; Kim, K.-J.; Joo, M. H.; Kim, T. H.; Yoon, S. S.; Chung, S. Molecular Orientation Dependence of Hole-Injection Barrier in Pentacene Thin Film on the Au Surface in Organic Thin Film Transistor. *Appl. Phys. Lett.* **2006**, *89*, 033504.
(16) Sun, Y.; Yin, Y.; Mayers, B. T.; Herricks, T.; Xia, Y. Uniform Silver Nanowires Synthesis by Reducing AgNO3 with Ethylene Glycol in the Presence of Seeds and Poly(vinyl pyrrolidone). *Chem. Mater.* **2002**, *14*, 4736−4745.
(17) Margulis, G. Y.; Christoforo, M. G.; Lam, D.; Beiley, Z. M.; Bowring, A. R.; Bailie, C. D.; Salleo, A.; McGehee, M. D. Spray Deposition of Silver Nanowire Electrodes for Semitransparent Solid-State Dye-Sensitized Solar Cells. *Adv. Energy Mater.* **2013**, *3*, 1657−1663.
(18) Lee, J.; Lee, P.; Lee, H.; Lee, D.; Lee, S. S.; Ko, S. H. Very Long Ag Nanowire Synthesis and Its Application in a Highly Transparent, Conductive and Flexible Metal Electrode Touch Panel. *Nanoscale* **2012**, *4*, 6408−6414.
(19) Kim, S. H.; Jang, M.; Yang, H.; Anthony, J. E.; Park, C. E. Physicochemically Stable Polymer-Coupled Oxide Dielectrics for Multipurpose Organic Electronic Applications. *Adv. Funct. Mater.* **2011**, *21*, 2198−2207.
(20) Maeda, T.; Kato, H.; Kawakami, H. Organic Field-Effect Transistors with Reduced Contact Resistance. *Appl. Phys. Lett.* **2006**, *89*, 123508.
(21) Hong, K.; Yang, S. Y.; Yang, C.; Kim, S. H.; Choi, D.; Park, C. E. Reducing the Contact Resistance in Organic Thin-Film Transistors by Introducing a PEDOT:PSS Hole-Injection Layer. *Org. Electron.* **2008**, *9*, 864−868.
(22) Newman, C. R.; Frisbie, C. D.; da Silva Filho, D. A.; Brédas, J.-L.; Ewbank, P. C.; Mann, K. R. Introduction to Organic Thin Film Transistors and Design of n-Channel Organic Semiconductors. *Chem. Mater.* **2004**, *16*, 4436−4451.
(23) Campbell, I.; Rubin, S.; Zawodzinski, T.; Kress, J.; Martin, R.; Smith, D.; Barashkov, N.; Ferraris. Controlling Schottky Energy Barriers in Organic Electronic Devices using Self-Assembled Monolayers. *J. Phys. Rev. B* **1996**, *54*, R14321−R14324.
(24) Campbell, I. H.; Kress, J. D.; Martin, R. L.; Smith, D. L.; Barashkov, N. N.; Ferraris, J. P. Controlling Charge Injection in Organic Electronic Devices using Self-Assembled Monolayers. *Appl. Phys. Lett.* **1997**, *71*, 3528.
(25) Hong, K.; Kim, S. H.; Yang, C.; Jang, J.; Cha, H.; Park, C. E. Improved n-type Bottom-Contact Organic Transistors by Introducing a Poly(3,4-ethylenedioxythiophene):Poly(4-styrene sulfonate) Coating on the Source/Drain Electrodes. *Appl. Phys. Lett.* **2010**, *97*, 103304.
(26) Käfer, D.; Ruppel, L.; Witte, G. Growth of Pentacene on Clean and Modified Gold Surfaces. *Phys. Rev. B* **2007**, *75*, 085309.
(27) Yang, H.; Yang, C.; Kim, S. H.; Jang, M.; Park, C. E. Dependence of Pentacene Crystal Growth on Dielectric Roughness for Fabrication of Flexible Field-Effect Transistors. *ACS Appl. Mater. Interfaces* **2010**, *2*, 391−396.

DOI: 10.1021/acsami.5b02610
ACS Appl. Mater. Interfaces 2015, 7, 14272−14278